ISSN 1027-5495. Functional Materials, 29, No.1 (2022), p. 567-575
doi:https://doi.org/10.15407/fm29.04.567 © 2022 — STC "Institute for Single Crystals"

Optical absorption of a composite with randomly distributed metallic inclusions of various shapes

A.V. Korotun, N.I. Pavlyshche

Department of Micro- and Nanoelectronics, National University "Zaporizhzhia Politechnic", 64 Zhukovsky Str., 69063 Zaporizhzhia, Ukraine

Recieved June 22, 2022

Size-frequency dependencies for the absorption coefficient of a composite with metallic nanoscale inclusions of various geometries have been studied within the concept of the equivalent ellipsoids of revolution. It has been established that the number of absorption coefficient maxima and their values depend on the shape of metallic inclusions while the spectral position of the maxima is determined by the material, and not by the shape of the inclusions. It has been shown that an increase in the attenuation results in a decrease in the absorption coefficient due to the invariability of the integral absorption coefficient.

Keywords: metal-dielectric nanocomposite, absorption coefficient, size dependence, surface plasmonic resonance, depolarization factors, effective relaxation time.

Оптичне поглинання композиту з випадково розподіленими металевими включеннями різної форми. *А.В. Коротун, Н.І. Павлище*

В рамках уявлень про еквівалентні еліпсоїди обертання досліджено розмірно-частотні залежності коефіцієнта поглинання композиту з металевими нанорозмірними включеннями різної геометрії. Встановлено, що кількість максимумів коефіцієнта поглинання та його величина залежать від форми металевих включень, тоді як спектральне положення максимумів визначається матеріалом, а не формою включень. Показано, що внаслідок незмінності інтегрального коефіцієнта поглинання зі збільшенням згасання коефіцієнт поглинання зменшується.

1. Introduction

The composite mediums based on dielectrics with metallic nanoparticles uniformly distributed over its volume (random or orderly), are under active study in recent years due to the large number of potential applications. This is due to the fact that such materials demonstrate new and interesting properties [1–3], which can differ significantly from initial properties of the material both the matrix and inclusions. One of the reasons of such differences is the effects of surface and quantum limitations at the nanoscale. In [4, 5] the occurrence of a resonance in the dielectric permittivity of the composite is assumed, and the position of the resonance depends both on the permittivity of the initial materials and on the volume content of nanoparticles in the composite and their geometry [3, 6]. The shape of the permittivity resonances in such composites coincides with the shape of the resonances of a three-dimensional sample, but the resonance is in the visible frequency range. In this case, the real part of the effective permittivity of the nanocomposites can vary over a wide range, from fairly large to negative [7, 8]. The required optical characteristics of the composite are formed as a result of excitation of the plasmonic resonance of nanoparticles, the frequency of which depends on the size and geometry of the nanoparticles [2, 9–12]. Variation in the size, shape, and orientation of nanoparticles opens up wide opportunities for controlling the optical properties of nanocomposites and their practical application [1, 2]. In particular, nanoparticles embedded in a

dielectric matrix, are used in the solar cells, sensors, LEDs and non-volatile memory devises [13-16]. The properties of nanoparticles embedded in a dielectric can be used to create materials with predetermined optical properties.

In [17], the size and shape effects on absorption and scattering properties of Au nanoparticles were studied. At the same time, it was shown that when changing the shape of nanoparticles from spheres to rods, the localized SPR peak shifts from the visible to the near-infrared region of the spectrum which makes such objects the potential candidates for in-vivo application [17].

In this regard, the purpose of this paper is to study the influence of inclusion geometry on the optical properties of metal-dielectric nanocomposites.

2. General theory

Let us use the relation for the absorption coefficient of a composite with ellipsoidal metal inclusions

$$\eta(\omega) = \frac{1}{3}\frac{\omega}{c}\beta\epsilon_{\mathrm{m}}^{\frac{3}{2}}\sum_{i=1}^{3}\frac{\epsilon_2^{(i)}(\omega)}{\left[\epsilon_{\mathrm{m}} + \mathcal{L}_i\left(\epsilon_1^{(i)}(\omega) - \epsilon_{\mathrm{m}}\right)\right]^2 + \left[\mathcal{L}_i\epsilon_2^{(i)}(\omega)\right]^2}, \tag{1}$$

where β is the content of nanoparticles in the composite; ϵ_{m} is matrix permittivity; c is the speed of light; ω is the frequency; $\mathcal{L}_i$ is the depolarization factors along the axes x, y, z ($i = x, y, z$). The real and imaginary parts of the dielectric function $\epsilon_1(\omega)$ and $\epsilon_2(\omega)$ in the Drude model are presented in the form

$$\epsilon_1^{(i)}(\omega) = \epsilon^{\infty} - \frac{\omega_p^2}{\omega^2 + \gamma_{\mathrm{eff}}^{(i)2}}, \quad \epsilon_2^{(i)}(\omega) = \frac{\omega_p^2\gamma_{\mathrm{eff}}^{(i)}}{\omega\left(\omega^2 + \gamma_{\mathrm{eff}}^{(i)2}\right)}. \tag{2}$$

In these formulae, ϵ^{∞} is the contribution of the ionic core to the permittivity; ω_p is the frequency of bulk plasmons; $\gamma_{\mathrm{eff}}^{(i)}$ is the diagonal component of the tensor of the effective relaxation rate determined by the following relation for nanoscale objects [18]

$$\gamma_{\mathrm{eff}}^{(i)} = \gamma_{\mathrm{bulk}} + \gamma_{\mathrm{s}}^{(i)} + \gamma_{\mathrm{rad}}^{(i)}, \tag{3}$$

where γ_{bulk} is the relaxation rate in a $3d$-metal; $\gamma_{\mathrm{s}}^{(i)}$ is the surface relaxation rate; $\gamma_{\mathrm{rad}}^{(i)}$ is the radiation damping rate.

Let us consider nanocomposites with particles-inclusions of such shapes as the strongly prolate and strongly oblate ellipsoids of revolution, as well as with particles of limiting shapes – rods, discs and spheres.

In the case of spheroidal, cylindrical and disk nanoparticles-inclusions, due to anisotropy, the permittivity is a diagonal tensor of the second rank

$$\epsilon = \begin{pmatrix} \epsilon^{\perp} & 0 & 0 \\ 0 & \epsilon^{\perp} & 0 \\ 0 & 0 & \epsilon^{\parallel} \end{pmatrix}, \tag{4}$$

where

$$\epsilon_1^{\perp(\parallel)}(\omega) = \epsilon^{\infty} - \frac{\omega_p^2}{\omega^2 + \gamma_{\mathrm{eff}}^{\perp(\parallel)2}}, \quad \epsilon_2^{\perp(\parallel)}(\omega) = \frac{\omega_p^2\gamma_{\mathrm{eff}}^{\perp(\parallel)}}{\omega\left(\omega^2 + \gamma_{\mathrm{eff}}^{\perp(\parallel)\,2}\right)}. \tag{5}$$

and the effective relaxation rate

$$\gamma_{\mathrm{eff}}^{\perp(\parallel)} = \gamma_{\mathrm{bulk}} + \gamma_{\mathrm{s}}^{\perp(\parallel)} + \gamma_{\mathrm{rad}}^{\perp(\parallel)}, \tag{6}$$

The ratios for the rates of radiation damping and surface relaxation in nanoparticles having the shape of an ellipsoid of revolution can be represented as [19, 20]

$$\gamma_{\mathrm{rad}}^{\perp(\parallel)} = \frac{2}{9\epsilon_0\sqrt{\epsilon_{\mathrm{m}}}}\left(\frac{\omega_p}{c}\right)^3 \frac{R_{\parallel}^2 R_{\perp}\mathcal{L}_{\perp(\parallel)}\sigma_{\perp(\parallel)}}{\sqrt{\epsilon^{\infty} + \left(\frac{1}{\mathcal{L}_{\perp(\parallel)}} - 1\right)\epsilon_{\mathrm{m}}}}, \tag{7}$$

$$\gamma_{\mathrm{s}}^{\perp(\parallel)} = \frac{\mathcal{L}_{\perp(\parallel)}\sigma_{\perp(\parallel)}}{\epsilon_0\left[\epsilon_{\mathrm{m}} + \mathcal{L}_{\perp(\parallel)}\left(1-\epsilon_{\mathrm{m}}\right)\right]}, \tag{8}$$

where ϵ_0 is the electric constant; $R_{\perp(\parallel)}$, $\mathcal{L}_{\perp(\parallel)}$, $\sigma_{\perp(\parallel)}$ are respectively, semi-axes of the ellipsoids of revolution, the depolarization factors and the diagonal components of the conductivity tensor, which correspond to the directions across and along the symmetry axes of a spheroid.

The frequency dependencies for the diagonal components of the conductivity tensor for spheroids have the form

$$\sigma_{\parallel} = \frac{9n_e e^2}{2m^*\omega}\left(\frac{\omega}{v_{s,\perp}}\right)^2 \frac{1}{e_p^3}\int\limits_{\frac{\omega}{v_{s,\perp}}}^{\frac{\omega}{v_{s,\parallel}}} \frac{dx}{x^4}\left[1-\left(\frac{\omega}{v_{s,\perp}x}\right)^2\right]^{\frac{1}{2}}\left\{1-\frac{2}{x}\sin x+\frac{2}{x^2}\left(1-\cos x\right)\right\}; \tag{9}$$

$$\sigma_{\perp} = \frac{9n_e e^2}{4m^*\omega}\left(\frac{\omega}{v_{s,\perp}}\right)^2 \frac{e_p^2-1}{e_p^3}\int\limits_{\frac{\omega}{v_{s,\perp}}}^{\frac{\omega}{v_{s,\parallel}}} \frac{dx}{x^4}\frac{1-\left(\frac{\omega}{v_{s,\parallel}x}\right)^2}{\left[1-\left(\frac{\omega}{v_{s,\perp}x}\right)^2\right]^{\frac{1}{2}}}\left\{1-\frac{2}{x}\sin x+\frac{2}{x^2}\left(1-\cos x\right)\right\}. \tag{10}$$

In formulae (9) and (10), x is the integration variable; the designations for the frequencies of the individual oscillations along the axes of spheroids are [19]:

$$v_{s,\parallel} = \frac{v_{\mathrm{F}}}{2R_{\parallel}}, \quad v_{s,\perp} = \frac{v_{\mathrm{F}}}{2R_{\perp}}. \tag{11}$$

where v_{F} is the Fermi speed of electrons.

Let us concretize the expressions (9) and (10) and write down the expressions for depolarization factors in the case of oblate ellipsoids of revolution:

$$\mathcal{L}_{\parallel} = \frac{1+e_p^2}{e_p^3}\left(e_p - \operatorname{arctg} e_p\right), \quad \mathcal{L}_{\perp} = \frac{1}{2}\left(1-\mathcal{L}_{\parallel}\right); \tag{12}$$

$$\sigma_{\parallel}\left(\omega\right) = \frac{9n_e e^2 v_{s,\parallel}}{16m^*\omega^2}\frac{1}{e_p^3}\left[e_p\left(1+2e_p^2\right) - \frac{\ln\left(e_p+\sqrt{1+e_p^2}\right)}{\sqrt{1+e_p^2}}\right]; \tag{13}$$

$$\sigma_{\perp}\left(\omega\right) = \frac{9n_e e^2 v_{s,\perp}}{32m^*\omega^2}\frac{1}{e_p^3}\left[e_p\left(2e_p^2-1\right)\sqrt{1+e_p^2} + \left(1+4e_p^2\right)\ln\left(e_p+\sqrt{1+e_p^2}\right)\right], \tag{14}$$

where $e_p = \sqrt{\left(R_{\perp}/R_{\parallel}\right)^2 - 1}$ is the eccentricity of the oblate spheroid.

The expressions for the depolarization factors and formulae (9) and (10) in the case of the prolate ellipsoids of revolution have the form

$$\mathcal{L}_{\parallel} = \frac{1-e_p^2}{2e_p^3}\left(\ln\frac{1+e_p}{1-e_p} - 2e_p\right), \quad \mathcal{L}_{\perp} = \frac{1}{2}\left(1-\mathcal{L}_{\parallel}\right); \tag{15}$$

$$\sigma_{\parallel}\left(\omega\right) = \frac{9n_e e^2 v_{s,\parallel}}{16m^*\omega^2}\frac{1}{e_p^3}\left[-e_p\left(1-2e_p^2\right) + \frac{\arcsin e_p}{\sqrt{1-e_p^2}}\right]; \tag{16}$$

$$\sigma_{\perp}\left(\omega\right) = \frac{9n_e e^2 v_{s,\perp}}{32m^*\omega^2}\frac{1}{e_p^3}\left[e_p\left(1+2e_p^2\right)\sqrt{1-e_p^2} - \left(1-4e_p^2\right)\arcsin e_p\right], \tag{17}$$

where $e_p = \sqrt{1-\left(R_{\perp}/R_{\parallel}\right)^2}$ is the eccentricity of the prolate spheroid.

3 A composite with inclusions of the spherical form

Let us concretize now the form of the expression for the absorption coefficient of a composite with inclusions of limited shape. In the case of spherical inclusions $\mathcal{L}_x = \mathcal{L}_y = \mathcal{L}_z = 1/3$ and

$$\eta(\omega) = \frac{9\omega}{c}\beta\epsilon_{\mathrm{m}}^{\frac{3}{2}}\frac{\epsilon_2(\omega)}{\left(\epsilon_1(\omega)+2\epsilon_{\mathrm{m}}\right)^2+\epsilon_2^2(\omega)}, \tag{18}$$

and surface and radiation components of the relaxation rate can be represented in the form [12]

$$\gamma_{\mathrm{s}} = \mathscr{A}_{\mathrm{sph}}(\omega, R)\frac{v_{\mathrm{F}}}{R}, \qquad \gamma_{\mathrm{rad}} = \mathscr{B}_{\mathrm{sph}}(\epsilon_{\mathrm{m}}, R)\frac{v_{\mathrm{F}}}{R}, \tag{19}$$

where

$$\mathscr{A}_{\mathrm{sph}}(\omega, R) = \frac{1}{4}\left(\frac{\omega_{\mathrm{p}}}{\omega}\right)^2\left[1-\frac{2\nu_s}{\omega}\sin\frac{\omega}{\nu_s}+\frac{2\nu_s^2}{\omega^2}\left(1-\cos\frac{\omega}{\nu_s}\right)\right]; \tag{20}$$

$$\mathscr{B}_{\mathrm{sph}}(\epsilon_{\mathrm{m}}, R) = \frac{1}{24\pi}\frac{V_0}{\sqrt{\epsilon_{\mathrm{m}}\left(2\epsilon_{\mathrm{m}}+\epsilon^{\infty}\right)}}\left(\frac{\omega_p}{c}\right)^3\left(\frac{\omega_p}{\omega}\right)^2, \tag{21}$$

$\nu_s = v_{\mathrm{F}}/2R$ is the frequency of individual oscillations, $V_0 = 4\pi R^3/3$ is the ball volume.

4 A composite with 1D-inclusions

The absorption coefficient for the nanocomposite with 1*D*-inclusions has the form

$$\eta(\omega) = \frac{1}{3}\frac{\omega}{c}\beta\epsilon_{\mathrm{m}}^{\frac{3}{2}}\left\{\frac{2\epsilon_2^{\perp}(\omega)}{\left[\epsilon_{\mathrm{m}}+\mathcal{L}_{\perp}\left(\epsilon_1^{\perp}(\omega)-\epsilon_{\mathrm{m}}\right)\right]^2+\left[\mathcal{L}_{\perp}\epsilon_2^{\perp}(\omega)\right]^2}+\right.$$
$$\left.+\frac{\epsilon_2^{\parallel}(\omega)}{\left[\epsilon_{\mathrm{m}}+\mathcal{L}_{\parallel}\left(\epsilon_1^{\parallel}(\omega)-\epsilon_{\mathrm{m}}\right)\right]^2+\left[\mathcal{L}_{\parallel}\epsilon_2^{\parallel}(\omega)\right]^2}\right\}. \tag{22}$$

The expressions for the absorption coefficients of composites with metallic inclusions of cylindrical and disc shapes can be obtained after passing to the limit from the corresponding relations for composites with inclusions in the form of oblong and oblate ellipsoids of revolution.

Note that since the properties of 1*D*-systems are described by relations for equivalent spheroids, it is convenient to use the effective aspect ratio of equivalent spheroids as a dimensional parameter instead of eccentricity. The aspect ratio, according to [21], can be determined from the condition of equality of the axial moments of inertia of a cylinder (spherocylinder) and a prolate spheroid or a disc and an oblate spheroid.

The axial moments of inertia for the cylinder, spheroid and oblong ellipsoid of revolution have the form

$$I_x^{\mathrm{cyl}} = \frac{m_{\mathrm{cyl}}}{12}\left(3r^2+l^2\right), I_z^{\mathrm{cyl}} = \frac{m_{\mathrm{cyl}}}{2}r^2, \tag{23, a}$$

$$I_x^{\mathrm{sphcyl}} = \pi r^5\rho_{\mathrm{sphcyl}}\left\{\frac{\delta}{6}\left(3+4\delta^2\right)+\frac{4}{3}\left(\frac{83}{320}+\left(\delta+\frac{3}{8}\right)^2\right)\right\}, \; I_z^{\mathrm{sphcyl}} = \pi r^5\rho_{\mathrm{sphcyl}}\left(\delta+\frac{8}{15}\right), \tag{23, b}$$

$$\delta = 1-\varrho \tag{23, c}$$

where r and l are, respectively, the radius and the length of the cylinder (spherocylinder), and m_{cyl} is the mass of the cylinder; ρ_{sphcyl} is the density of the material of the spherocylinder;

$$I_x^{\mathrm{ell}} = \frac{m_{\mathrm{ell}}}{5}\left(a^2+b^2\right), \quad I_z^{\mathrm{ell}} = \frac{2m_{\mathrm{ell}}}{5}b^2, \tag{24}$$

where m_{ell} is the mass of the ellipsoid.

Using the relation

$$\frac{I_x^{\mathrm{ell}}}{I_z^{\mathrm{ell}}} = \frac{I_x^{\mathrm{cyl}}}{I_z^{\mathrm{cyl}}}, \tag{25}$$

and introducing the designations

$$\varrho_{\text{eff}} = \frac{b}{a}, \quad \varrho = \frac{2r}{l}, \quad \varrho = \frac{2r}{l-2r}, \tag{26}$$

where ϱ is the aspect ratio for the cylinder and spherocylinder, one obtains

$$\varrho_{\text{eff}} = \frac{\sqrt{3}}{2}\varrho, \quad \varrho_{\text{eff}} = \left(1 + \frac{4\delta}{3}\frac{\delta^2 + 2\delta + \frac{3}{4}}{\delta + \frac{8}{15}}\right)^{-\frac{1}{2}}, \tag{27}$$

In the case of a disc and an oblong ellipsoid of revolution, the first relation (27) is also true, but the expressions for ϱ_{eff} and ϱ have the form:

$$\varrho_{\text{eff}} = \frac{a}{b}, \quad \varrho = \frac{D}{H}, \tag{28}$$

where D and H is the diameter and the height of the disc.

Calculating integrals (9) and (10) for both cases without taking into account the oscillating terms in comparison with the term in parentheses, we obtain the expressions for the diagonal components of the conductivity tensor.

- for a prolate spheroid equivalent to the cylinder (spherocylinder)

$$\sigma_{\perp(\parallel)} = \frac{9}{16}\epsilon_0\left(\frac{\omega_p}{\omega}\right)^2 \nu_{s,\perp}\mathscr{F}_{\perp(\parallel)}\left(\varrho_{\text{eff}}\right), \tag{29}$$

where

$$\mathscr{F}_{\perp}\left(\varrho_{\text{eff}}\right) = \left(1-\varrho_{\text{eff}}^2\right)^{-\frac{3}{2}}\left\{\varrho_{\text{eff}}\left(\frac{3}{2}-\varrho_{\text{eff}}^2\right)\sqrt{1-\varrho_{\text{eff}}^2} + \left(\frac{3}{4}-\varrho_{\text{eff}}^2\right)\ln\left(\varrho_{\text{eff}} + \sqrt{1-\varrho_{\text{eff}}^2}\right)\right\}; \tag{30}$$

$$\mathscr{F}_{\parallel}\left(\varrho_{\text{eff}}\right) = \left(1-\varrho_{\text{eff}}^2\right)^{-\frac{3}{2}}\left\{\frac{\pi}{2} - \arcsin\varrho_{\text{eff}} + \varrho_{\text{eff}}\left(1-2\varrho_{\text{eff}}^2\right)\sqrt{1-\varrho_{\text{eff}}^2}\right\};$$

- for an oblate spheroid equivalent to a disc, $\sigma_{\perp(\parallel)}$ has the form (29), but $\mathscr{F}_{\perp(\parallel)}\left(\varrho_{\text{eff}}\right)$ is determined by formulas

$$\mathscr{F}_{\perp}\left(\varrho_{\text{eff}}\right) = \frac{1}{2}\left(\varrho_{\text{eff}}^2-1\right)^{-\frac{3}{2}}\left\{\varrho_{\text{eff}}\left(2\varrho_{\text{eff}}^2-3\right)\sqrt{\varrho_{\text{eff}}^2-1} + \left(4\varrho_{\text{eff}}^2-3\right)\ln\left(\varrho_{\text{eff}} + \sqrt{\varrho_{\text{eff}}^2-1}\right)\right\}; \tag{31}$$

$$\mathscr{F}_{\parallel}\left(\varrho_{\text{eff}}\right) = \left(\varrho_{\text{eff}}^2-1\right)^{-\frac{3}{2}}\left\{\varrho_{\text{eff}}\left(2\varrho_{\text{eff}}^2-1\right)\sqrt{\varrho_{\text{eff}}^2-1} - \ln\left(\varrho_{\text{eff}} + \sqrt{\varrho_{\text{eff}}^2-1}\right)\right\}.$$

Substituting expressions (29) into formulae (7) and (8), we obtain general expressions for the rates of surface relaxation and radiation damping

$$\gamma_{\text{s}}^{\perp(\parallel)} = \frac{9}{16}\frac{\mathcal{L}_{\perp(\parallel)}}{\epsilon_{\text{m}} + \mathcal{L}_{\perp(\parallel)}\left(1-\epsilon_{\text{m}}\right)}\nu_{s,\perp}\left(\frac{\omega_p}{\omega}\right)^2\mathscr{F}_{\perp(\parallel)}\left(\varrho_{\text{eff}}\right); \tag{32}$$

$$\gamma_{\text{rad}}^{\perp(\parallel)} = \frac{V}{8\pi}\frac{\mathcal{L}_{\perp(\parallel)}}{\sqrt{\epsilon_{\text{m}}\left[\epsilon^{\infty} + \left(\frac{1}{\mathcal{L}_{\perp(\parallel)}}-1\right)\epsilon_{\text{m}}\right]}}\nu_{s,\perp}\left(\frac{\omega_p}{c}\right)^3\left(\frac{\omega_p}{\omega}\right)^2\mathscr{F}_{\perp(\parallel)}\left(\varrho_{\text{eff}}\right). \tag{33}$$

We will use the latter relations to calculate the frequency dependencies for the absorption coefficient of a composite with metallic 1D-inclusions using formula (22).

Table 1. Parameters of metallic inclusions (see, e.g., [12, 22] and references therein)

Metal	Parameter			
	r_s / a_0	m^* / m_e	ϵ^∞	γ_{bulk}, 10^{13} s^{-1}
Al	2.07	1.48	0.7	12,50
Cu	2.11	1.49	12.03	3,70
Au	3.01	0.99	9.84	3,45
Ag	3.02	0.96	3.7	2,50

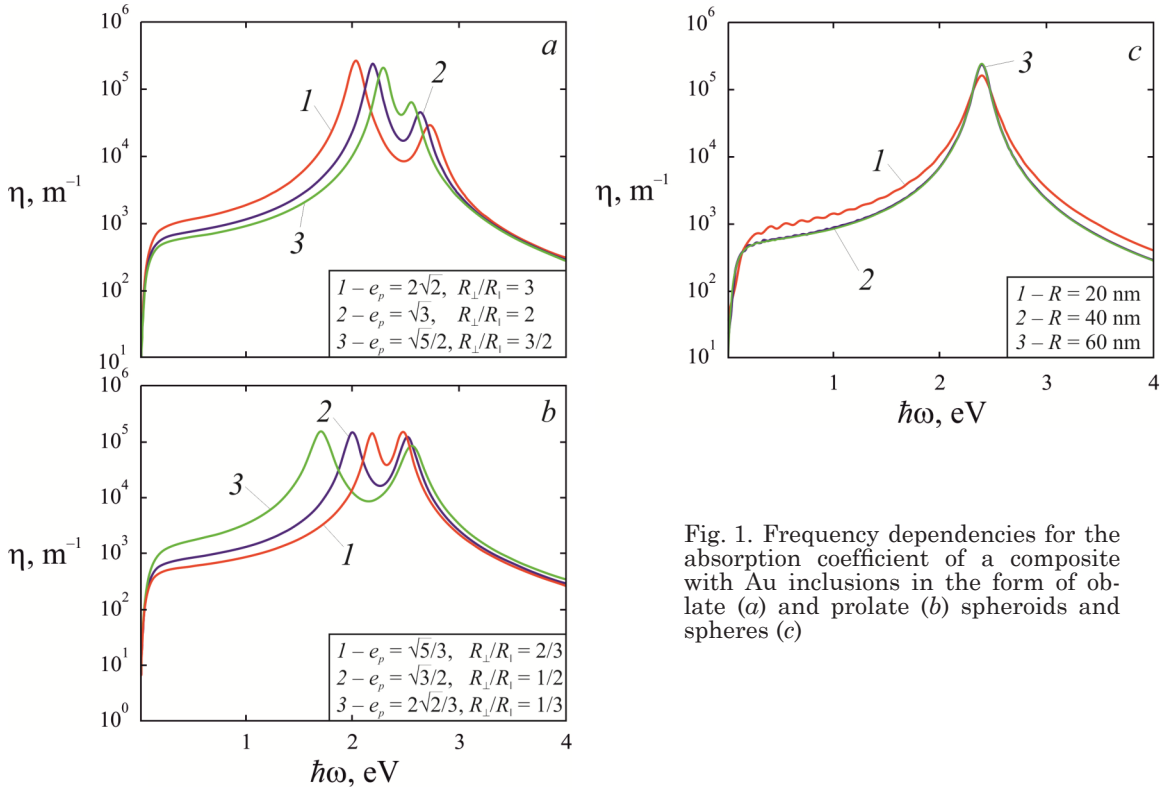

Fig. 1. Frequency dependencies for the absorption coefficient of a composite with Au inclusions in the form of oblate (*a*) and prolate (*b*) spheroids and spheres (*c*)

5 Calculation results and discussion

Calculations of frequency dependencies for the absorption coefficient were performed for composites of Teflon ($\epsilon_m = 2.3$) with inclusions of various metals with different geometry. The parameters of materials of the inclusions are given in Table 1.

Figure 1 shows the frequency dependencies for the absorption coefficient of the composite with gold nanoparticles of spheroidal and spherical shapes and different sizes. It should be pointed out that a decrease in the eccentricity of inclusions in the shape of oblate spheroids (Fig 1, *a*) results in a "blue" shift of the first maximum and a decrease in its numerical value. On the contrary, the second maximum shows a "red" shift of the maximum and an increase in its value. At the same time, the second maxima are much lower than the first ones. The same shifts of the first and second maxima are characteristic of composites with oblong spheroidal inclusions. (Fig. 1, *b*). The only difference from the previous case is that the values of the first and the second maximums are close. At the same time, for a composite with spherical inclusions (Fig. 1c), the frequency dependence of the absorption coefficient has one maximum, and curves 1–3 differ insignificantly in the case of inclusions of different radii.

Figure 2 shows similar frequency dependencies for the absorption coefficient of composites with spheroidal and spherical inclusions of fixed sizes of various metals. In the case of inclusions of an oblate spheroidal shape (Fig. 2a), for Au, Cu, and Ag inclusions, the second maximum is smaller

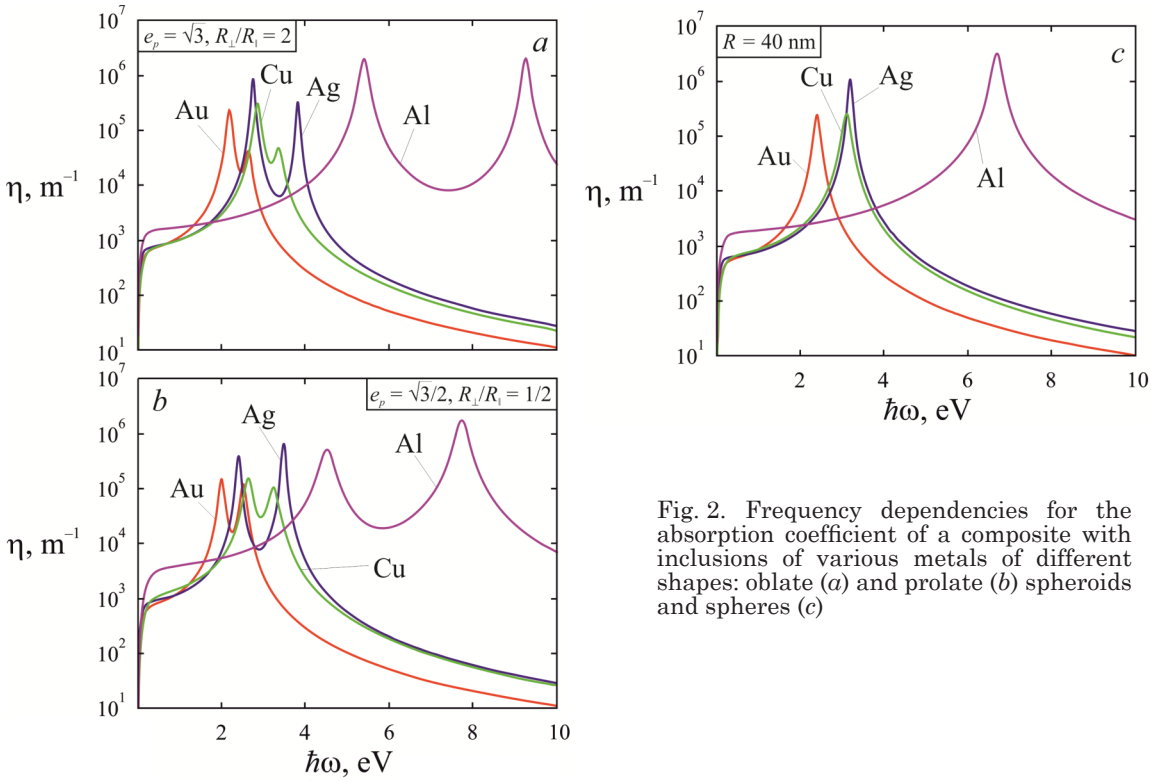

Fig. 2. Frequency dependencies for the absorption coefficient of a composite with inclusions of various metals of different shapes: oblate (*a*) and prolate (*b*) spheroids and spheres (*c*)

than the first maximum; while for Al inclusions, they are almost the same. For composites with inclusions of an oblong spheroidal shape (Fig. 2, *b*) the second maxima are smaller for Au and Cu inclusions, however, they are larger than the first maxima for Ag and Al inclusions. For composites with the spherical inclusions of various metals, the absorption coefficient shows one maximum (Fig. 2, *c*). Its position $\eta_{\max}(\omega)$ for the composites with inclusions of various metals is determined by the frequency of bulk plasmons and the contribution of the crystal lattice to the permittivity.

Figure 3 shows the graphs of the frequency dependencies for the absorption coefficients of composites with gold 1*D*-inclusions in the form of cylinders of finite length and discs. It should be noted that the curves $\eta(\omega)$ of the composites with such inclusions are qualitatively similar and quantitatively close. However, while for composites with cylindrical inclusions the values of the maxima of the absorption coefficient are close, for composites with inclusions in the form of disks, the value of the second maximum is much less than the value of the first maximum. This fact becomes clear if one considers cylinders and disc as the limiting forms of the oblong and oblate spheroids.

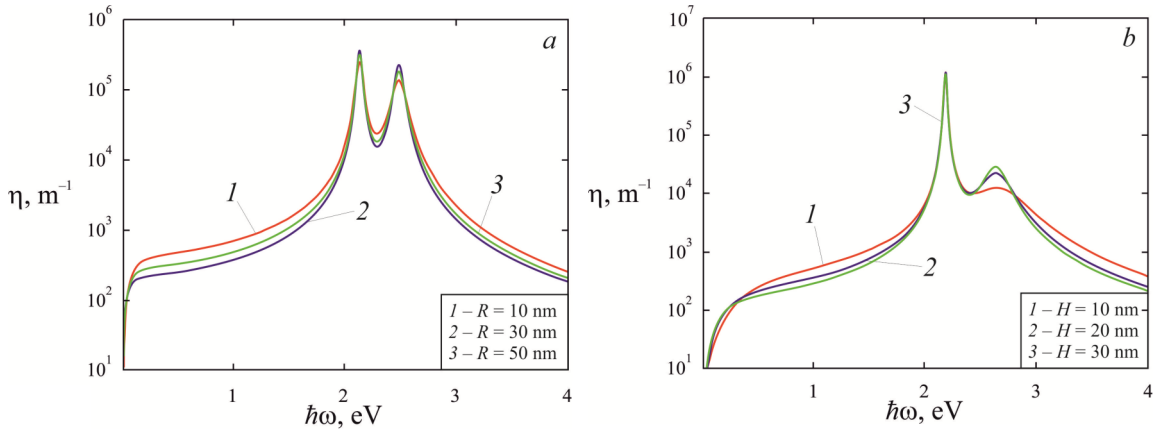

Fig. 3. Frequency dependencies for the absorption coefficient of a composite with metallic Au 1*D*-inclusions of different sizes: *a* – cylinders (c_{eff}=0.5); *b* – discs ($\varrho_{eff} = 2$)

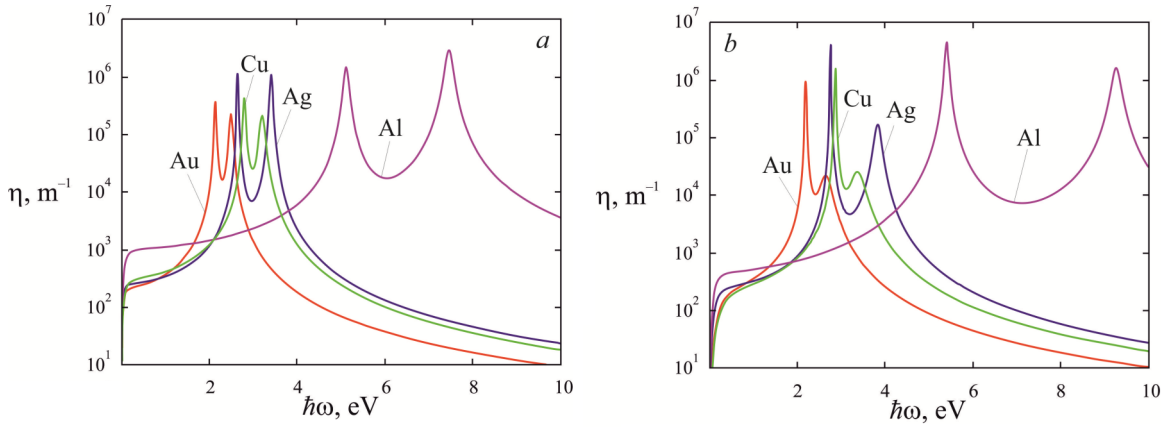

Fig. 4. Frequency dependencies for the absorption coefficient of a composite with inclusions of different metals: (*a*) cylindrical with c_{eff}=0.5 and $R = 30$ nm and (*b*) discs with $\varrho_{eff} = 2$ and $H = 20$ nm

Figure 4 shows the frequency dependencies for the absorption coefficients of the composites with the similar inclusions of different metals of the fixed size. Note that the ratio between the values of the first and second maxima for the composites with cylinders (Fig. 4, *a*) and discs (Fig. 4, *b*) is exactly the same as in the case of the inclusions of different metals in the form of oblong and oblate spheroids (Fig. 2, *a* and 2, *b*).

In conclusion, we note that all the maxima of the frequency dependencies of the absorption coefficient for composites with metallic inclusions, which are shown in Fig. 1 – 4, are observed at $\omega = \omega_{sp}$ for the spherical inclusions and at $\omega = \omega_{sp}^{\perp(\parallel)}$ for the inclusions in the shape of oblong and oblate spheroids, rods and discs.

For a composite with the spherical inclusions at $\omega = \omega_{sp}$,

$$\epsilon_1\left(\omega_{sp}\right) + 2\epsilon_{\rm m} = 0 \text{ and } \eta\left(\omega_{sp}\right) = \frac{9\beta}{c}\epsilon_{\rm m}^{\frac{3}{2}}\frac{\omega_{sp}}{\epsilon_2\left(\omega_{sp}\right)}, \tag{34}$$

and for the inclusions of other geometry at $\omega = \omega_{sp}^{\perp(\parallel)}$

$$\epsilon_1^{\perp(\parallel)}\left(\omega_{sp}^{\perp(\parallel)}\right) = -\frac{1-\mathcal{L}_{\perp(\parallel)}}{\mathcal{L}_{\perp(\parallel)}}\epsilon_{\rm m}. \tag{35}$$

The maxima of the absorption coefficients

$$\eta\left(\omega_{sp}^{\perp}\right) = \frac{1}{3}\frac{\omega_{sp}^{\perp}}{c}\beta\epsilon_{\rm m}^{\frac{3}{2}}\left\{\frac{2}{\mathcal{L}_{\perp}^2\epsilon_2^{\perp}\left(\omega_{sp}^{\perp}\right)} + \frac{\epsilon_2^{\parallel}\left(\omega_{sp}^{\perp}\right)}{\left[\epsilon_{\rm m} + \mathcal{L}_{\parallel}\left(\epsilon_1^{\parallel}\left(\omega_{sp}^{\perp}\right) - \epsilon_{\rm m}\right)\right]^2 + \left[\mathcal{L}_{\parallel}\epsilon_2^{\parallel}\left(\omega_{sp}^{\perp}\right)\right]^2}\right\} \tag{36}$$

and

$$\eta\left(\omega_{sp}^{\parallel}\right) = \frac{1}{3}\frac{\omega_{sp}^{\parallel}}{c}\beta\epsilon_{\rm m}^{\frac{3}{2}}\left\{\frac{2\epsilon_2^{\perp}\left(\omega_{sp}^{\parallel}\right)}{\left[\epsilon_{\rm m} + \mathcal{L}_{\perp}\left(\epsilon_1^{\perp}\left(\omega_{sp}^{\parallel}\right) - \epsilon_{\rm m}\right)\right]^2 + \left[\mathcal{L}_{\perp}\epsilon_2^{\perp}\left(\omega_{sp}^{\parallel}\right)\right]^2} + \frac{1}{\mathcal{L}_{\parallel}^2\epsilon_2^{\parallel}\left(\omega_{sp}^{\parallel}\right)}\right\}. \tag{37}$$

It follows from the formulae (34), (36) and (37) that an increase in the attenuation (ϵ_2 for the spherical particles or $\epsilon_2^{\perp(\parallel)}$ – for nonspherical) results in a decrease in the value $\eta\left(\omega_{sp}\right)$ (or $\eta\left(\omega_{sp}^{\perp(\parallel)}\right)$). This result is characteristic of the absorption of light by metal nanoparticles and is due to the fact that an increase in the damping of plasma oscillations leads to an increase in the half-width of the surface plasmon resonance $\Delta\omega_{sp}$. Due to the fact that the integral absorption coefficient is a constant value, $\eta_{\Sigma} = \eta\left(\omega_{sp}\right)\Delta\omega_{sp} = \text{const}$, the maximum absorption coefficient $\eta\left(\omega_{sp}\right)$ will decrease with increasing attenuation, while the half-width of the resonance should increase, since $\Delta\omega_{sp} \sim \epsilon_2$.

6. Conclusions

The size-frequency dependencies for the absorption coefficient of composites with metallic inclusions in the form of oblong and oblate spheroids and their limiting forms – spherical nanoparticles,

nanodiscs and nanorods have been obtained. The size dependence for the absorption coefficient is determined by the size dependencies for the depolarization factors and effective relaxation times. In order to determine these size dependencies for the cylinders and discs we used the concept of equivalent ellipsoids of revolution, the optical properties of which coincide with the optical properties of nanocylinders and nanodiscs.

The results of calculating the frequency dependences of the absorption coefficient indicate the existence of a relationship between the magnitude and number of maxima and the geometry of the inclusions. In the case of spherical inclusions, the absorption coefficient has one maximum, while for inclusions of other forms, two maxima are observed. This is due to the fact that during the deformation of the sphere, the dipole plasmonic mode splits into the transverse and longitudinal plasmonic modes.

It has been shown that in the case of inclusions in the form of oblate spheroids and discs the magnitudes of the second maxima of the absorption coefficient are smaller than the first maxima for Au, Cu, Ag, while the both maxima are almost equal for Al. In the case of elongated spheroids and nanorods, the values of the second maxima can be both smaller (inclusions of Au and Cu) and larger (inclusions of Ag and Al) than the values of the first maxima. It has been established that the position of the maxima of the absorption coefficient for inclusions of different metals is almost independent of geometry of the inclusions and is determined by the frequency of bulk plasmons and by the contribution of ion core into the permittivity of the materials of inclusion particles.

It has been demonstrated, that a decrease in the absorption coefficient with an increase in the attenuation due to the constancy of the integral absorption coefficient is the particularity of light absorption by the composite with nanoscale inclusions.

References

1. H. Ning, Composites and Their Properties, Chiba University, Chiba, Japan (2012).
2. I.M. Krishchenko, É.G. Manoilov, S.A. Kravchenko et. al., *Theor. Experim. Chem.*, **56**, 67 (2020).
3. A.A. Koval, A.V. Korotun, Yu.A. Kunitsky et. al., Electrodynamics of plasmon effects in nanomaterials, Kyiv: "Naukova dumka", 2021; 344 p. [in Ukrainian].
4. A.N. Oraevskii, I.E. Procenko, *Pisma v JETF*, **72**, 641, (2000) [in Russian].
5. A.N. Oraevskii, I.E. Procenko, *Kvantova elektronika*, **31**, 252, (2001) [in Russian].
6. O.A. Yeshchenko, I.S. Bondarchuk, A.A. Alexeenko et. al., *Funct. Mater.*, **20**, 357 (2013).
7. W. Cai, U.K. Chettiar, A.V. Kildishev et. al., *Nat. Photonics*, **1**, 224, (2007).
8. O.A. Zaimidoroga, V.N. Samoilov, S.E. Procenko, *Fiz. el. chastic i atom. yadra*, **33**, 101, (2002) [in Russian].
9. V.V. Klimov, Nanoplasmonics, FL: CRC Press, Taylor and Francis Group, Boca Raton, (2014).
10. K.L. Kelly, E. Coronado, L.L. Zhao et. al., *J. Phys. Chem. B.*, **107**, 668 (2003).
11. N. Toropov, T. Vartanyan, *Compreh. Nanosc. Nanotechn*, **1-5**, 61 (2019).
12. A.V. Korotun, N.I. Pavlyshche, *Phys. Met. Metallogr.*, **122**, 941 (2021).
13. G. Chakraborty, A. Sengupta, F. Requejo et. al., *J. Appl. Phys.*, **109**, 064504, (2011).
14. T. Cesca, B. Kalinic, C. Maurizio et. al., *Phys. Status Solidi B*, **252**, 119, (2015).
15. H. Liu, D.A. Ferrer, F. Ferdousi et. al., *Appl. Phys. Lett.* **95**, 203112 (2009).
16. D. Munthala, A. Mangababu, S.V.S. Nageswara Rao et. al., *J. Appl. Phys.*, **130**, 044301 (2021).
17. P.K. Jain, K.S. Lee, I.H. El-Sayed et. al., *J. Phys. Chem. B*, **110**, 7238, (2006).
18. C.F. Bohren, D.R. Huffman, Absorption and scattering of light by small particles, John Wiley & Sons (2008).
19. N.I. Grigorchuk, P.M. Tomchuk, *Phys. Rev. B.*, **84**, 085448 (2011)
20. N.I. Grigorchuk, *J. Opt. Soc. Am. B*, **29**, 3404 (2012).
21. D. Constantin, *Eur. Phys. J. E*, **38** 116 (2015).
22. A.V. Korotun, A.A. Koval, V.I. Reva, *J. Appl. Spectrosc.*, **86**, 606 (2019).